

General Relativistic Radiative Transfer: Emission from Accreting Black Holes in AGN

Kinwah Wu¹ *, Steven V. Fuerst¹, Khee-Gan Lee^{1,2} and Graziella Branduardi-Raymont¹

¹ Mullard Space Science Laboratory, University College London, Holmbury St Mary, Surrey, RH5 6NT, United Kingdom

² Department of Physics and Astronomy, University College London, Gower Street, London, WC1E 6BT, United Kingdom

Abstract We present two covariant radiative transfer formulations, and apply them to calculate emission from relativistic accretion flows around black holes. The first formulation is for situations with only line-of-sight absorption and emission, while the second formulation is for situations where scattering is important. We use the first formulation to calculate emissions from opaque accretion disks and tori around black holes absorbed by high-velocity cloudlets. Our calculations show the importance of effects due to space-time curvature, relativistic motions of the emitters and absorbers, and external line-of-sight absorption. We find that external absorption tends to take away line fluxes at energies red-ward of the line-centre energy. In its presence, emission lines from geometrically thin opaque relativistic accretion disks may not have broad asymmetric double-peak profiles: in some situations the lines may appear to be narrow, sharp and blue-shifted. We also find that geometric effects are important for thick accretion disks (accretion tori). When viewed at high inclination angles, the inner surface of an accretion torus can be self-occulted. As the most highly red-shifted and blue-shifted emissions are blocked, emission lines from an opaque accretion torus would suffer less broadening and the line intensities are less boosted. These lines may have single-peak profiles, but their line centres are slightly red-shifted. We apply the radiative transfer formulation to calculate emission lines from optically thin and semi-opaque accretion tori, and generalise it to calculate continua emission, such as the reflection spectra, of accretion disks. The second covariant radiative transfer formulation, which is based on a moment method, is used to calculate the emissions from accretion tori with the opacity being dominated by electron scattering. We demonstrate that the formulation is applicable for a wide range of optical depths appropriate for accretion tori around black holes.

Key words: accretion, accretion disks — black hole physics — galaxies: active — line: profiles — radiative transfer — relativity

1 INTRODUCTION

The strong X-rays from active galactic nuclei (AGN) are believed to be powered by accretion of material into a central supermassive black hole. The black hole's gravity curves the space-time, modifying the hydrodynamics of the accretion flow around the hole and altering the transportation of the radiation from the accreting gas.

Emission lines from thin accretion disks around compact objects are expected to show two peaks (Smak 1969), which correspond to emission from the two sides of the accretion disks with approaching and receding line-of-sight velocities. For non-relativistic accretion flows, the peaks are symmetric when line-of-sight absorption is negligible. Symmetric double-peak optical lines have been found in cataclysmic variables (see

* E-mail: kw@mssl.ucl.ac.uk

Williams 1983) and some black-hole X-ray binaries (see e.g. Wu et al. 2001). For the accretion onto a black hole, the flow speeds can be very high near the event horizon and may reach the speed of light, causing the frequency of the radiation from the infalling gas to be Doppler shifted, and boosting the intensity. However, the gravitational field near the black-hole event horizon is also very strong. It causes time dilation, which in turn shifts the radiation to lower frequencies. We would therefore expect that X-ray lines emitted from the inner accretion disk around a black hole will have profiles more complex than the symmetric double-peak profiles such as those of the optical lines from a non-relativistic Keplerian accretion flow. Calculations (e.g. Fabian et al. 1989; Laor 1991; Fanton et al. 1997; Reynolds et al. 1999) have shown that X-ray lines from a geometrically thin relativistic accretion disk around a black holes generally have very broad, asymmetric profiles. At moderate view inclination angles, say at 45° , the blue peak is sharp and tall, but the red peak is shorter and has an extensive red wing. At higher inclination angles, the line is even broader but the red peak becomes less distinguishable. Emission lines of such profiles have been observed in the X-ray spectra of several AGN, with the Fe $K\alpha$ line of MCG-6-30-15 as the best known example (Tanaka et al. 1995).

Such emission lines from relativistic accretion disks around black holes can be calculated using a number of methods (see e.g. discussions in Fuerst & Wu (2004)). In most calculations, a simple model for the accretion disk is assumed: usually the disk is Keplerian, geometrically infinitely thin and optically thick. The disk inner rim is set to the last stable orbit of particles, while the emissivity of the line is parametrised by a radial power law, with the strongest intensity at the inner disk rim and decreasing outwards. Continuum emission is usually not considered, and self-absorption and line-of-sight or absorption are ignored. (To date the two studies including resonant absorption/scattering are Ruszkowski & Fabian (2000) and Fuerst & Wu (2004).) These studies have provided a theoretical framework for the interpretation of the broad X-ray lines seen in the AGN spectra (see review by Fabian et al. 2000). Advancements in instrumentation result in spectra with good S/N and high resolutions, and there now exist a demand for more sophisticated line profile calculations that treat the relevant physics properly.

Here we investigate radiative transfer in black-hole environments and how it affects the X-ray spectra of AGN. We present a covariant radiative transfer formulation which takes into account line-of-sight absorption and emission (Sect. 2), following which we discuss the kinematics of the emitters and absorbers, and the resonant absorption/scattering condition for the photons (Sect. 3). We then construct accretion-disk and accretion-torus models and calculate the line and continuum emission (Sects. 4, 5 and 6). This is followed by a discussion on the importance of effects due to geometry, line-of-sight absorption and self-absorption in the context of AGN spectroscopy. Finally we also discuss briefly a moment formulation for radiative transfer in the presence of scattering (Sect. 7).

2 COVARIANT RADIATIVE TRANSFER EQUATION

The classical radiative transfer equation reads

$$\left[\frac{1}{c} \frac{\partial}{\partial t} + (\hat{n} \cdot \nabla) \right] I_\nu = -\kappa_\nu I_\nu + j_\nu + \iint d\nu' d\Omega' \sigma(\nu, \nu') I_{\nu'}(\Omega'), \quad (1)$$

where I_ν is the specific intensity, \hat{n} is the light propagation unit vector, κ_ν is the absorption coefficient, j_ν is the emissivity and σ is the scattering cross section. It describes the propagation of radiation in flat space-time. The equation needs to be modified to a covariant form, in order to calculate emission from high-speed accreting flows near a black-hole event horizon.

A covariant radiative transfer equation can be derived from the conservation of particles and their phase-space density, i.e. Liouville's Theorem. For a space-time specified by a metric $g_{\alpha\beta}$, with the interval given by $d\tau = g_{\alpha\beta} dx^\alpha dx^\beta$, an expression for the equation of radiative transfer in the absence of scattering is

$$\frac{d\mathcal{I}}{d\lambda} = -k_\alpha u^\alpha|_\lambda [-\chi_o(x^\beta, \nu)\mathcal{I} + \eta_o(x^\beta, \nu)] \quad (2)$$

(Baschek et al. 1997), where λ is the affine parameter, k^α is the four-momentum of photon, and u^α is the four-velocity of the medium. The Lorentz intensity is defined as $\mathcal{I} \equiv I_\nu/\nu^3$; χ_o and η_o are the corresponding Lorentz invariant effective absorption coefficient and emissivity. (Here and hereafter the subscript ‘‘o’’ denotes evaluation at the local rest frame.) Along a light ray,

$$\frac{d}{d\lambda} = k_\alpha \frac{\partial}{\partial x^\alpha} - \Gamma_{\beta\gamma}^\alpha k^\beta k^\gamma \frac{\partial}{\partial k^\alpha}, \quad (3)$$

where $\Gamma_{\beta\gamma}^{\alpha}$ is the affine connection. Hence, the covariant radiative transfer equation can also be expressed as

$$k_{\alpha} \frac{\partial \mathcal{I}}{\partial x^{\alpha}} - \Gamma_{\beta\gamma}^{\alpha} k^{\beta} k^{\gamma} \frac{\partial \mathcal{I}}{\partial k^{\alpha}} = -k_{\alpha} u^{\alpha} |_{\lambda} [-\chi_{\circ}(x^{\beta}, \nu) \mathcal{I} + \eta_{\circ}(x^{\beta}, \nu)] \quad (4)$$

(Fuerst & Wu 2004). The same expression can be derived alternatively from the Boltzmann Equation (Lindquist 1966).

Solving the transfer equation (Eq. 2) along a ray yields

$$\begin{aligned} \mathcal{I}(\lambda) = & \mathcal{I}(\lambda_0) \exp \left(\int_{\lambda_0}^{\lambda} d\lambda' k_{\alpha} u^{\alpha} |_{\lambda'} \chi_{\circ}(\lambda', \nu_{\circ}) \right) \\ & - \int_{\lambda_0}^{\lambda} d\lambda' k_{\alpha} u^{\alpha} |_{\lambda'} \eta_{\circ}(\lambda', \nu_{\circ}) \exp \left(\int_{\lambda'}^{\lambda} d\lambda'' k_{\alpha} u^{\alpha} |_{\lambda''}, \chi_{\circ}(\lambda'', \nu_{\circ}) \right) \end{aligned} \quad (5)$$

with “0” denoting initial conditions. This solution will be used in our numerical ray-tracing calculations in Sections 3, 4 and 5.

3 EQUATIONS OF MOTION FOR PARTICLES AND RESONANT ABSORPTION OF PHOTONS

Before proceeding to solve the radiative transfer equations, we need to specify the absorption coefficient and emissivity, i.e. we need models for the emitters and for the line-of-sight absorbers. For the emitters we consider two models: thin Keplerian accretion disks and accretion tori, which will show the effects of the geometry. For the line-of-sight absorbers, we assume that the emission is absorbed by virialised clouds that are thermally cold but kinematically hot.

We also need to specify the structure of the space-time on which the world lines of photons, emitters and absorbers propagate. We consider flows near black holes, and the space-time is given by a Kerr metric in Boyer-Linquist coordinates:

$$\begin{aligned} d\tau^2 = & \left(1 - \frac{2Mr}{\Sigma} \right) dt^2 + \frac{4aMr \sin^2 \theta}{\Sigma} dt d\phi - \frac{\Sigma}{\Delta} dr^2 \\ & - \Sigma d\theta^2 - \left(r^2 + a^2 + \frac{2a^2 Mr \sin^2 \theta}{\Sigma} \right) \sin^2 \theta d\phi^2, \end{aligned} \quad (6)$$

where $\Sigma = r^2 + a^2 \cos^2 \theta$ and $\Delta = r^2 - 2Mr + a^2$. The parameters M and a are the mass and spin of the central black hole respectively ($a = 0$ for Schwarzschild black holes and $a = 1$ for maximally rotating Kerr black holes). Here and hereafter we adopt the convention $c = G = k_B = 1$ for the speed of light, gravitational constant and Boltzmann constant.

The Lagrangian for the free particles is

$$\begin{aligned} \mathcal{L} = & -\frac{1}{2} \left[\left(1 - \frac{2Mr}{\Sigma} \right) \dot{t}^2 + \frac{4aMr \sin^2 \theta}{\Sigma} \dot{t} \dot{\phi} - \frac{\Sigma}{\Delta} \dot{r}^2 \right. \\ & \left. - \Sigma \dot{\theta}^2 - \left(r^2 + a^2 + \frac{2a^2 Mr \sin^2 \theta}{\Sigma} \right) \sin^2 \theta \dot{\phi}^2 \right] \end{aligned} \quad (7)$$

(with $\dot{x}^{\alpha} \equiv dx^{\alpha}/d\lambda$), from which we can derive the equations of motions of photons and gas particles in a Keplerian disk (see e.g. Reynolds et al. 1999; Fuerst 2005). For particles under an external force, the equation of motion is

$$\frac{d^2 x^{\alpha}}{d\lambda^2} + \Gamma_{\beta\gamma}^{\alpha} \dot{x}^{\beta} \dot{x}^{\gamma} = a^{\alpha}, \quad (8)$$

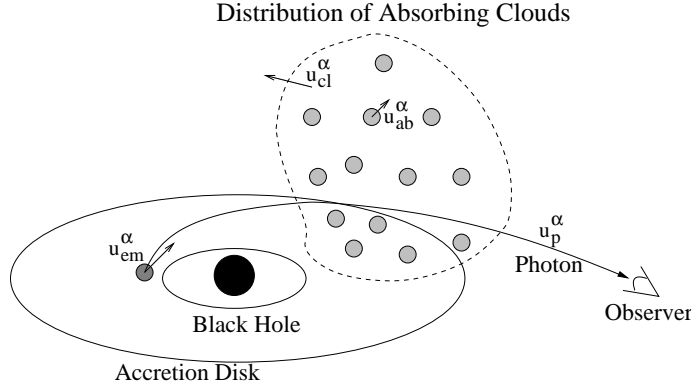


Fig. 1 A schematic illustration of the setting of the absorbing cloud model in the radiative transfer calculation. The gravity of the central black hole determines the space-time metric. The quantities u_p^α , u_{em}^α , u_{ab}^α and u_{cl}^α are 4-velocities for the photons, the emitters, the absorbing particles and the cloud bulk flow respectively. The emitters are on the surface of an accretion disk, as shown, or an accretion torus.

where a^α is the four-acceleration corresponding to external (non-gravitational) forces. In the construction of the model accretion torus we use a parametric velocity law to determine a^α . We assume a parametric model with the angular velocity profile:

$$\Omega = \frac{1}{(r \sin \theta)^{3/2} + a} \left(\frac{r_k}{r \sin \theta} \right)^n. \quad (9)$$

The parameter r_k is the radius in the equatorial plane at which the gas particles have a Keplerian velocity. The parameter n determines the aspect ratio of the model accretion torus.

We assume that the lines are resonantly scattering. As there are not many photons scattered into the line energies along the line-of-sight, we approximate the resonant scattering process by resonant absorption. We do not consider the effects due to energy redistribution explicitly. The line absorption coefficient is given by

$$\chi_o = -\frac{2\pi C \sigma}{E_{line}^2} \iint d\mu dp p^2 k_\alpha u^\alpha \exp\left(-\frac{E}{\Theta}\right) \delta\left(\frac{k_\alpha u^\alpha + E_{line}}{E_\gamma}\right), \quad (10)$$

where $\mu \equiv \cos \theta$, p and E are the momentum and energy of an absorbing particles in the bulk flow rest frame, Θ is characteristic thermal temperature of the particles, σ is the absorption cross-section parameter (to be determined later), E_{line} is the absorption line rest frame and E_γ is the photon energy in the bulk flow rest frame. The normalisation constant

$$C = \frac{1}{4\pi} \left(\frac{m}{\Theta} \right) \frac{N}{m^3 K_2(m/\Theta)}, \quad (11)$$

where N is the number density of absorbing clouds and m is the average mass of the clouds, and $K_2(\dots)$ is the modified Bessel Function of order 2. It can be shown that the absorption coefficient can be expressed as

$$\chi_o = \frac{N\sigma}{2K_2(m/\Theta)} \left[\frac{1}{2} \left(\frac{E_\gamma}{E_{line}} + \frac{E_{line}}{E_\gamma} \right) + \frac{\Theta}{m} \right] \exp \left[-\left(\frac{m}{2\Theta} \right) \left(\frac{E_\gamma}{E_{line}} + \frac{E_{line}}{E_\gamma} \right) \right] \quad (12)$$

(Fuerst & Wu 2004; Fuerst 2005). The parameter σ now corresponds to the absorption cross-section per cloud. We consider a power-law parametrisation: $N\sigma = \sigma_0 r^{-\beta}$, where σ_0 is a proportionality constant determined by the density and opacity scales. We set the index $\beta = 3/2$ without losing generality, as it is straightforward to modify the calculations to obtain results for other values.

The geometrical setting for the radiative transfer calculations is as shown in Figure 1. A ray-tracing algorithm is used. For the cases without line-of-sight absorption, the energy-shift images of accretion disks

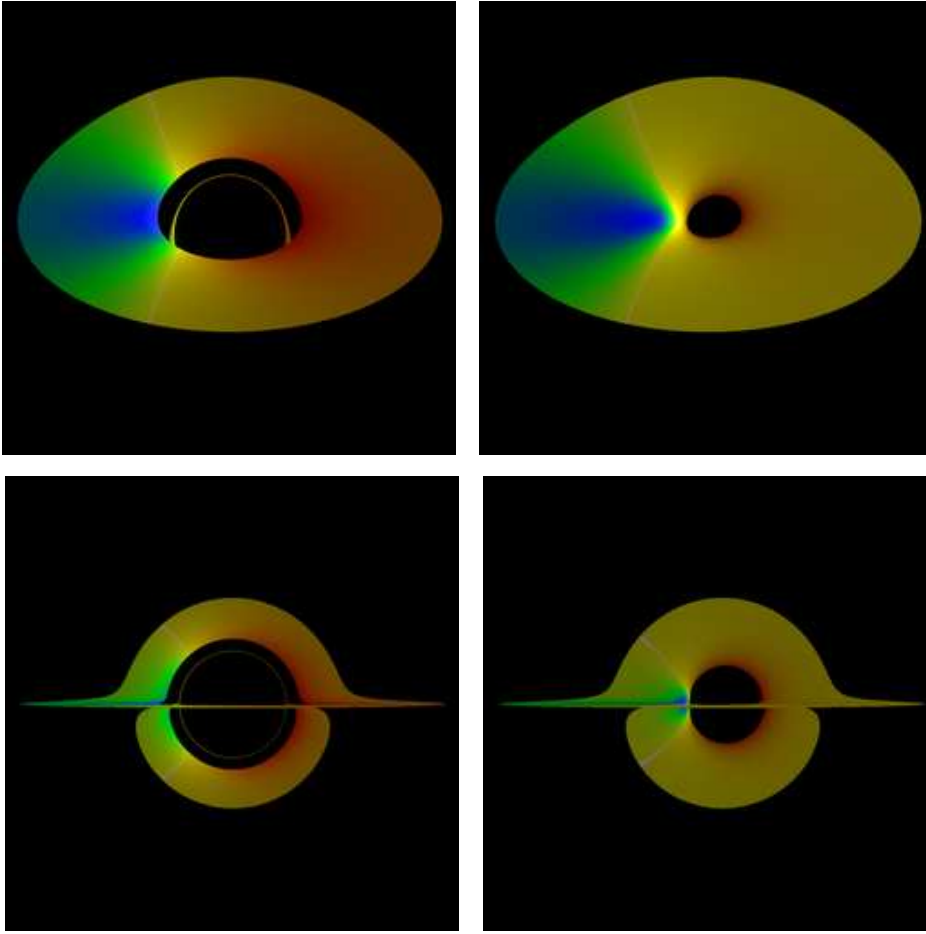


Fig. 2 False-colour images of Keplerian accretion disks around Schwarzschild black holes (left column) and Kerr black holes with $a = 0.998$ (right column), viewed at inclinations of 60° (upper panels) and 89° (lower panels). The outer disks are truncated at $20 r_g$. Blue represents energy up-shift, and red energy down-shift viewed by a distant observer. The separatrix (where there is zero energy shift) are denoted by grey lines.

or tori projected onto the sky-plane are first generated. The line emissions from each surface element in the disk/torus images are then calculated with proper correction for the energy shifts and weighting of the specific intensity. Finally the emissions are summed to produce the spectra. For the cases with absorption, the photon trajectories are first determined and the relative energy-shifts along the trajectories are calculated. The covariant radiative transfer equation is then solved along the trajectories to determine the line and continuum spectra.

4 EMISSION FROM OPAQUE ACCRETION DISKS AND TORI

In the calculations of line emission from the accretion disks and accretion tori, we first generate disk/torus images displaying the energy shift of the photons originating from the disk surface elements that reach the distant observer. The lines are the sum of contributions of line emission from all "visible" surface elements for an assumed line profile function in the local rest frame. The procedures to calculate continuum emission are similar. For isotropic continuum emission, we need to replace the local line profile function by a local

continuum spectrum. For anisotropic continuum emission, we must first determine the pitch angles of the photons, relative to the normal of the emitting surface, that reach the observer. We then calculate the local rest-frame angle dependent spectrum for each disk surface element.

4.1 Geometrically Thin Accretion Disks

We now consider a simple case, where the lines are emitted from a geometrically thin Keplerian accretion disk. The disk is optically thick, but internal absorption is not treated explicitly. The emission is assumed to be generated on the two disk surfaces, and there is no line-of-sight absorption. Figure 2 shows the projected energy-shift images of disks around Schwarzschild ($a = 0$) and Kerr black holes (with $a = 0.998$) onto the sky-plane. The photons emitted from different locations suffer different degrees of energy shifts when propagating outwards to a distant observer. The shapes of the disks are distorted because of gravitational lensing.

In the calculations we have assumed that the inner disk radius is set by the last stable particle orbit, which is $6 r_g$ for Schwarzschild black holes and is $1.23 r_g$ for Kerr black holes with $a = 0.999$ (where r_g is the gravitational radius). The small inner radius for the accretion disks around Kerr black holes implies that the high-order lensed images are obscured and will not be visible, when viewed at low inclination angles. However, if the viewing inclinations are high enough, the second and higher-order images will become visible, as the photon trajectories are now outside the disk outer rim.

Emissions from the inner regions of a thin disk around a maximally rotating Kerr black hole are red-shifted at all viewing inclination angles. This is contrary to the case of Schwarzschild black holes, where there are regions at the inner disk boundary from which the emissions are severely blue-shifted, at sufficiently high viewing inclination angles.

Figure 3 shows two examples of emission lines from geometrically thin accretion disks with contribution from the first-order disk image only. Absorption is not included in these calculations. The characteristic asymmetric double-peak profile (Fabian et al. 1989) is clearly seen in the case of Schwarzschild black holes. An asymmetric broad profile is also seen in the case of Kerr black holes, but the two peaks are not easy to distinguish. In both cases, the red wing is very extensive, but the blue peak is taller and it appears as if the blue side is truncated.

Absorption can significantly modify an emission line profile. Its effects are well manifested in the P Cygni line profiles for emission from optically thick outflows, and asymmetric optical lines are seen in spectra of some black-hole binaries (see e.g. Wu et al. 2001). The calculations for absorbed emissions from

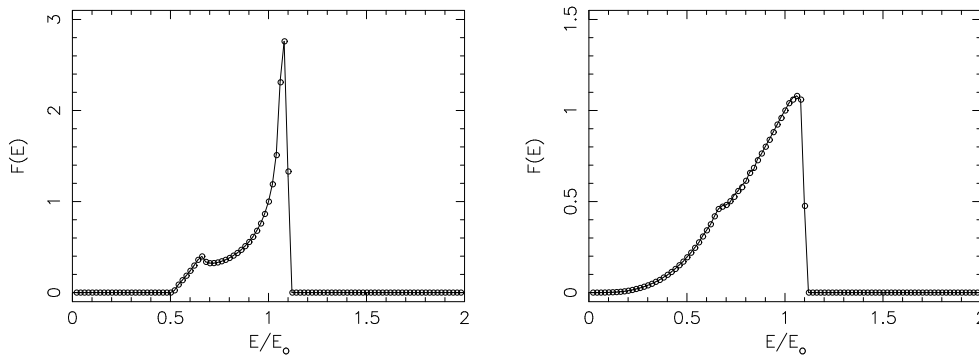


Fig. 3 The profiles of emission lines calculated from first-order images of thin Keplerian accretion disks around a Schwarzschild black hole (top) and a Kerr black hole with $a = 0.998$ (bottom). The view inclinations are 45° and the outer disk radius is set to be $10 r_g$. The emissivity of the line decreases radially outward with R following a power law with an index of -3 . The normalisation of the line is such that the flux $F(E) = 1$ at $E/E_0 = 1$, where E_0 is the rest line-centre energy. The solid lines correspond to results obtained from semi-analytic calculations following the method described in Fanton et al. (1997). The circles correspond to results from our numerical ray-tracing calculations (Adapted from Fuerst & Wu (2004).)

inner accretion disks around black holes are complicated by the following: (1) The absorbing gas clouds close to the black hole may have very high speeds. (2) The line profile function depends on the relative speeds of the absorbers and the emitters as well as the structure of space-time. (3) The line absorption opacity profile is not symmetric with respect to the line-centre rest-frame energy, because of Doppler shifts and time dilation.

Figure 4 shows disk power-law continua with photons resonantly absorbed/scattered by a line, where the line-of-sight cloudlets are in relativistic motion as viewed by the observer. The kinematics of the cloudlets are determined using the prescription described in Section 2. The calculations show that the absorption line profile depends strongly on the line-centre rest-frame optical depth. System parameters such as viewing orientation and the black-hole spin, however, play a less significant role in shaping the lines. (See Fuerst & Wu (2004) for absorption line profiles with various system parameters.)

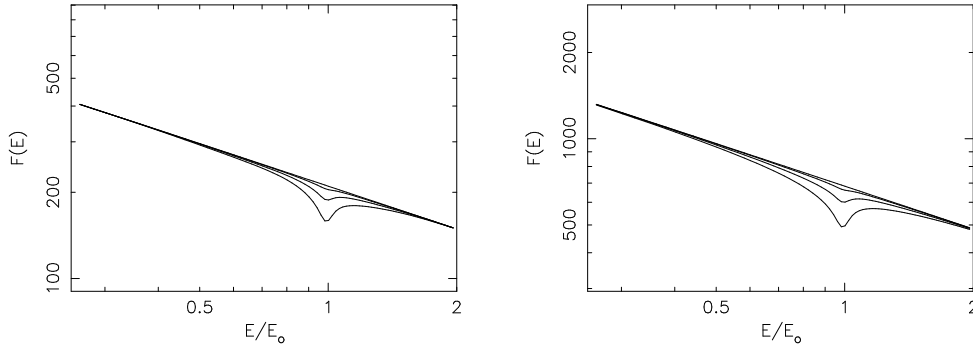


Fig. 4 Absorption line profiles in power-law continua from accretion disks around Kerr black holes with $a = 0.998$, at viewing inclination angle of 45° (left) and 85° (right). Virialised clouds above the accretion disk provide the line-of-sight absorption. The values of the parameters σ_0 specifying the absorption optical depth are 0, 0.05, 0.2 and 0.5 (curves from top to bottom in each panel). (Adopted from Fuerst & Wu (2004).)

Figure 5 shows disk spectra where the line and the continuum are resonantly absorbed/scattered by line-of-sight cloudlets. The combinations of various system parameters give rise to a variety of line profiles. When absorption is negligible, the lines preserve the characteristic asymmetric double-peak profiles as those shown in the left panel in Figure 3. In the presence of strong line-of-sight absorption, the lines may lose the double-peak disk signature completely. For the extreme cases, the line fluxes at the red-wing energies can be absorbed to below the level of the underlying continuum. In spite of this, the blue wing of the line is not affected much by absorption. It is worth noting that at some moderate absorption optical depths the red wing is absorbed with its fluxes at the same level as the nearby continuum. In this situation the line will appear as if it is intrinsically narrow and centred at a higher energy.

Note that resonant absorption/scattering effects were also investigated previously by Ruszkowski & Fabian (2000) in a resistive setting in which the line-of-sight material was assumed to be a rotating “hemisphere”. Moreover, the radiative transfer equation was not solved explicitly but instead the Sobolev approximation was used. In this study, the motion of the absorbing material is determined by a specified dynamical process, and the resonant absorption/scattering is considered explicitly and microscopically using a phenomenological approach. Nevertheless, similar relativistic effects were seen in the two studies, in particular the asymmetry in the absorption line profiles.

4.2 Accretion Tori

Figure 6 shows the images of an accretion torus around a Kerr black hole with $a = 0.998$ viewed at inclination angles of 60° and 89° . The boundary surface of the torus is determined using the method described in Fuerst & Wu (2004) and Fuerst (2005). The index n of the parametric velocity power-law (in Equation (9)) is chosen such that the aspect ratio of the torus is similar to those of the tori obtained by numerical

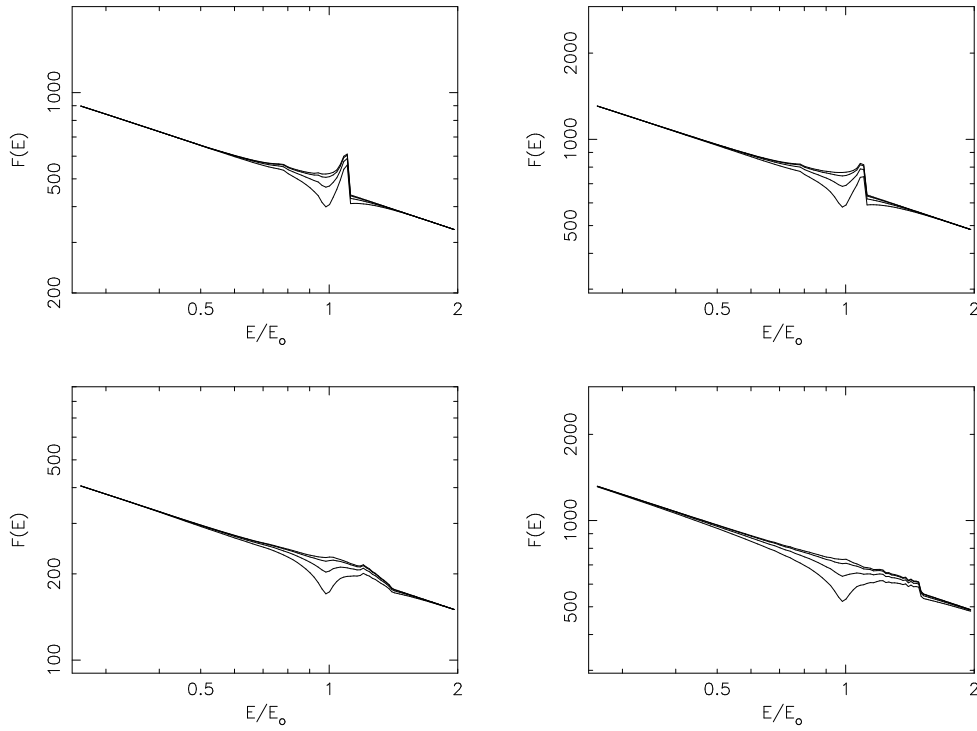


Fig. 5 Line and continuum emission from accretion disks around Schwarzschild black holes (left column) and Kerr black holes with $a = 0.998$ (right column), viewed at inclination of 45° (top panels) and 85° (bottom panels). The value of the parameters σ_0 are 0, 0.05, 0.2 and 0.5 (curves from top to bottom in each panel). The index of the radial power-law line emissivity is -2 . (Adopted from Fuerst & Wu (2004).)

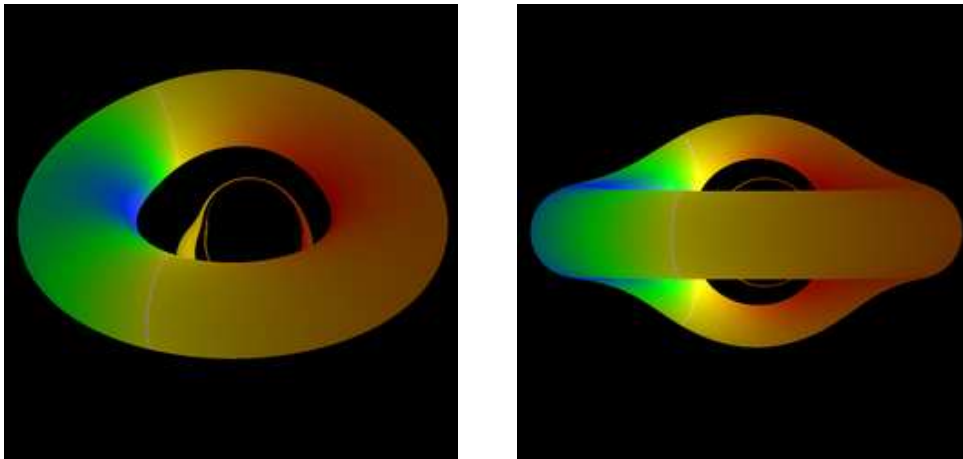


Fig. 6 False-colour images of an accretion torus around a Kerr black hole (with $a = 0.998$) viewed at inclination angles of 60° (left panel) and 89° (right panel). The boundary surface of the torus is determined as described in the text and in Fuerst & Wu (2005). The velocity law parameters are $n = 0.21$ and $r_k = 12$. For these parameter values the aspect ratio is similar to the accretion tori obtained by the numerical simulation of Hawley & Balbus (2002). Blue represents energy up-shift, and red energy down-shift viewed by a distant observer. The separatrices (where there is no energy shift) are denoted by grey lines.

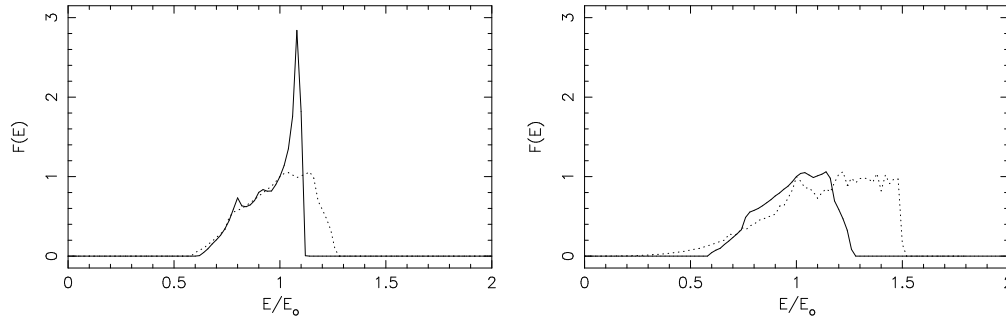


Fig. 7 Left panel: profile of emission lines from an accretion torus around a Kerr black hole with $a = 0.998$, viewed at inclination angles of 45° (solid line) and 85° (dotted line). The index of the radial power-law line emissivity is -2 . Right panel: A comparison of profiles of emission lines from an accretion torus (solid line) and a thin Keplerian accretion disk (dotted line) viewed at inclination angle of 85° . The outer radius of the thin accretion is truncated at $20 r_g$. (Adapted from Fuerst & Wu (2004).)

simulations of Hawley & Balbus (2002). Typically, for accretion tori similar to that in Figure 6, the radius of the inner boundary is about $8.5 r_g$, for $r_k = 12 r_g$. (For tori around Schwarzschild black holes, the inner boundary radius is about $12 r_g$ if setting $r_k = 15 r_g$.)

It is noticeable that the inner boundary radius of the torus in Figure 6 is significantly larger than the inner radius of the corresponding accretion disk (cf $1.23 r_g$ for disks around black holes with $a = 0.998$). A consequence of a large inner radius for the torus is that emission from some parts of the inner torus surface is blue-shifted while emission from some other parts is red-shifted. Another consequence is that the high-order images are visible at low viewing inclination angles. In addition, self-occultation can occur in tori. At high viewing inclination angles, a significant fraction of the inner torus surface, where the most highly red-shifted and blue-shifted emissions originate, is obscured because of the thickness of the torus. All these are at variance with the case of the thin accretion disks. The upper surface of a thin accretion disk is always invisible, and for disks around maximally rotating black holes the emission from the inner disk rim is red-shifted regardless of viewing inclination.

The occultation of the inner torus boundary surface, together with a large radius for the inner boundary, have significant effects on the emission line profiles. The effects can be easily seen by comparing the line profiles of tori and thin disks at different viewing inclination angles. At sufficiently low viewing inclination angles where self-occultation does not occur, a torus will give asymmetric double-horn lines (left panel, Figure 7). If we set the inner radius of an accretion disk the same as the radius of the inner boundary surface of the torus, the profile of the disk line and the profile of the torus line are almost identical. However, for viewing inclinations close to 90° , the difference between the lines from a torus and a thin disk becomes obvious (right panel, Figure 7). The line of the torus lacks the strong blue-shifted emission. Its red wing is slightly less extensive than the red wing of the disk line. The overall appearance of a torus line is still broad and more symmetric than that of its counterpart for the thin disk.

5 RELATIVISTIC REFLECTION SPECTRA FROM THIN DISKS

Here we consider geometrically thin accretion disks and determine the spectra of its Compton-reflection of the power-law component. We assume that the intensity decreases radially outward following a power-law with an index of -3 . As reflection emissions are anisotropic, we need to determine the pitch angles and energy shifts of the emerging photons from the disk surface, and calculate the reflection spectrum of each disk surface element. We consider the model reflection spectra given by Magdziarz & Zdziarski (1995), which can be generated using the astronomical X-ray spectral software package XSPEC. The reflection spectra for all surface elements (with corrections for relativistic effects) are summed to obtain the reflected spectra of the entire accretion disk. The algorithm of the calculations is presented in Lee et al. (2005).

Figure 8 (left panel) shows the reflection spectra of a thin Keplerian accretion disk around a Schwarzschild black hole viewed at inclinations of 1° , 45° and 85° . For comparison of the shifts in the edge features between the three cases we show the quotient spectra, normalised to the spectrum of the disk with an inclination angle of 45° , in the same figure (right panel). As shown, the sharp straight absorption edges which are normally present in reflection spectra are smeared and smoothed. The edge smearing and smoothing are caused by the combination of two processes. Firstly, the energy shifts of the emerging photons are different for different disk surface elements; secondly photons from different surface elements that reach the observer have different pitch angles. The location of the edges are shifted because of the energy shifts of the photons. The degree of edge smearing and edge shifting vary with the viewing inclination angle. Its relative dependence on the disk orientation is manifested in the spikes and wiggles in the quotient spectra.

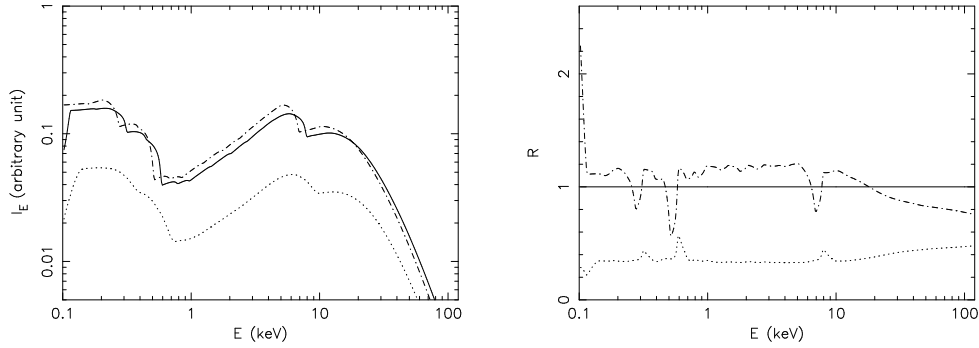


Fig. 8 Left panel: Reflection spectra of a geometrically thin Keplerian accretion disk around a Schwarzschild black hole viewed at inclination angles of 1° (dot-dashed line), 45° (solid line) and 85° (dotted line). The index of the line emissivity radial power-law is -3 . The intensity I_E is in arbitrary unit. Right panel: The corresponding quotient spectra of the three spectra in the left panel. The normalised intensity R is such that it is unity for the spectrum in the case where the inclination viewing angle is 45° (solid line). Spectra for the inclination angles of 1° and 85° are represented by dot-dashed and dotted lines respectively.

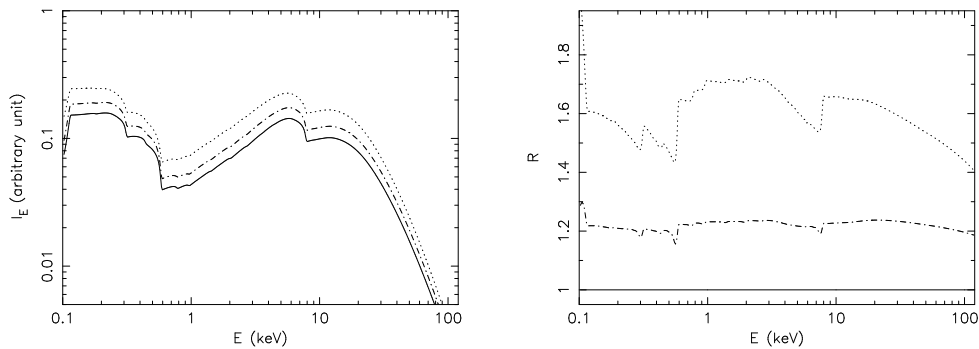


Fig. 9 Left panel: Reflection spectra of geometrically thin Keplerian accretion disks around black holes with $a = 0$ (solid line), 0.5 (dot-dashed line) and 0.998 (dotted line) viewed at an inclination angle of 45° . The index of the line emissivity radial power-law is -3 . The intensity I_E is in arbitrary unit. Right panel: The corresponding quotient spectra of the spectra in the left panel. The normalised intensity R is such that it is unity for the spectrum in the case of the Schwarzschild black hole (solid line). Spectra for black holes with $a = 0.5$ and 0.998 are represented by dot-dashed and dotted lines respectively.

Figure 9 shows the reflection spectra (left panel) and corresponding quotient spectra (right panel) of disks around black holes with different rotational rates ($a = 0, 0.5$ and 0.998). The viewing inclinations of the disks are fixed to 45° . The edges of the spectra are smeared and smoothed as in Figure 8. However, the features in the quotient spectra are not identical to those in Figure 8. In particular, the edges here are smeared towards the low energies. This can be explained as follows. In the disk model that we employ, the location of the inner disk boundary is assumed to be the last stable orbit, which is set by the spin of the black hole. For a radial emissivity power-law of index -3 , most of the emission originates from the inner disk region, where gravitational red-shift is severe and dominates other relativistic effects. The cause of smearing in the spectra is therefore mainly due to different weights in the contribution of the strong gravitationally red-shifted emission.

To date the two representative studies of relativistic reflection spectra are Martocchia, Karas & Matt (2000) and Dovciak, Karas & Yaqoob (2004). The numerical scheme that we use in our calculations is the same as the (powerful) convolution scheme described in Dovciak, Karas & Yaqoob (2004). The convolution kernel in our calculations is still based on the reflection model provided by XSPEC. However, we have employed a radiative transfer formulation (Fuerst & Wu 2004) which is more versatile than the standard Laor (1991) method in the relativistic calculations. This gives us the advantages that the calculations can easily be generalised for disks with substantial thickness (e.g. the opaque tori discussed in a later section), and that reflection from high-order images can be calculated (Fuerst et al., in preparation).

6 EMISSION FROM SEMI-TRANSPARENT ACCRETION TORI

6.1 Density Structure of the Tori

We now show various transfer effects when the accretion tori are transparent (or partially transparent) to the radiation. Following Abramowicz, Jaroszynski & Sikora (1978) and Kozłowski, Jaroszynski & Abramowicz (1978) we can construct model accretion tori with internal structure. We assume that the accretion torus are composed of a perfect fluid. The total pressure of the fluid is the sum of the thermal gas pressure and the radiation pressure, i.e. $P = P_{\text{gas}} + P_{\text{rad}}$, where

$$P_{\text{gas}} = \frac{\rho k_{\text{B}} T}{\mu m_{\text{H}}} = \bar{\beta} P, \quad (13)$$

$$P_{\text{rad}} = \frac{4}{3} \sigma T^4 = (1 - \bar{\beta}) P, \quad (14)$$

with T as the gas thermal temperature, ρ the gas density, k_{B} the Boltzmann constant, σ the Stefan-Boltzmann constant, μ the mean molecular weight, m_{H} the hydrogen mass, and $\bar{\beta}$ the parameter specifying the relative contribution to the total pressure by the thermal gas. We consider a polytropic equation of state, $P = \kappa \rho^\Gamma$, where κ is a constant to be determined and Γ is the polytropic index. The momentum equation is then

$$P_{,\beta} g^{\alpha\beta} = - \left(\rho + \frac{\Gamma}{\Gamma - 1} P \right) a^\alpha. \quad (15)$$

The density structure of the torus is given by

$$\frac{\partial \rho}{\partial x^\alpha} = -g_{\alpha\beta} a^\beta \left(\frac{\rho^{2-\Gamma}}{\kappa \Gamma} + \frac{\rho}{\Gamma - 1} \right). \quad (16)$$

It follows that for radiation dominated tori with $\Gamma = 4/3$,

$$\frac{\partial \ln \rho}{\partial x^\alpha} = 3g_{\alpha\beta} a^\beta \left(\frac{1}{4\kappa \rho^{1/3}} + 1 \right) \quad (17)$$

(Fuerst 2005; Fuerst & Wu 2005), where

$$\kappa = \left[\frac{45(1 - \bar{\beta})}{\pi^2 (\mu m_{\text{H}} \bar{\beta})^4} \right]^{1/3} \quad (18)$$

(see e.g. Bowers & Deeming 1984). The equation has only two non-trivial components, in the \hat{r} and $\hat{\theta}$ directions. For a Kerr space-time, the corresponding components of the four-acceleration a^α are given by

$$g_{rr}a^r = -r\dot{\phi} + \left[\frac{\dot{t}}{r} (1 - a\Omega) \right]^2, \quad (19)$$

$$g_{\theta\theta}a^\theta = -\sin\theta \cos\theta \left[\frac{2r}{\Sigma} \left(at - (r^2 + a^2) \dot{\phi} \right)^2 + \Delta\dot{\phi}^2 \right]. \quad (20)$$

We solve for ρ by evaluating the line integral from (r_k, θ) with a central density $\rho = \rho_c$ to the specific location (r, θ) .

6.2 Emission from the Tori

The radiative transfer formulation presented in Section 2 is applicable to calculate the emission from accretion disks as well as accretion tori which have density, temperature and velocity structures. Figure 10 shows two examples of the calculations of emission from structured accretion tori. The left panel shows the surface brightness of a transparent torus. The spin parameter of the central black hole is $a = 0.998$. The aspect ratio is the same as those for the optically thick case in the previous section. The emission of the torus is due to neutral Fe $K\alpha$ and $K\beta$ lines. The emissivity of the Fe $K\beta$ line is set to be 14% of that of the $K\alpha$ line (see Hölzer et al. 1997). The density of the torus is sufficiently low that the optical depths of the two lines are negligible. We therefore ignore self-absorption in the radiative transfer calculations. The torus is visually distorted, with the far side gravitationally lensed to appear much larger than the near side. High-order images are visible, because of the low optical depths of the emission. Due to Doppler boosting, the emission from the torus half where the emitters have proceeding line-of-sight velocities is amplified, but the half where the emitters have receding line-of-sight velocities is dimmed. A limb effect, caused by density (and hence emissivity) variations with the minor radius of the torus, is visible.

The right panel of Figure 10 shows the surface brightness image of a semi-opaque accretion torus. The spin parameter of the central black hole and the aspect ratio of the torus are the same as those of the torus in the left panel. The emission of the torus consists of a neutral Fe $K\alpha$, a neutral $K\beta$ line, a free-free continuum and a power law (with spectral index of -2.5). Both the line and continuum have substantial optical depths. Self-absorption cannot be neglected and is treated explicitly in the calculations. As can be seen, the torus is not completely transparent, and its near side obscures the high-order images. At higher inclination angles, self-occultation also occurs. Doppler boosting effects are visible, but are less obvious in comparison with the transparent torus. The semi-opaque torus is also limb darkened. The cause is, however, not the same as that of the transparent torus. In addition to density variations, temperature variations also play an important role here. Oblique rays leaving the torus surface tend to sample the emission from a skin layer near the limb surface, while perpendicular rays leaving the torus surface sample greater depths inside the torus, where the temperature is higher. Thus, the torus trunk will appear brighter and the torus limb will appear darker.

The lines from transparent and semi-opaque tori also show asymmetric double-peak profiles at low viewing inclination angles. At high viewing inclination angles the profiles of lines from a semi-opaque torus would resemble those of the lines from an opaque torus.

7 RADIATIVE TRANSFER WITH SCATTERING: MOMENT FORMULATIONS

The radiative transfer formulation in the previous sections considers line-of-sight emission and absorption but omits scattering. When the scattering process is important, we need to take into account the photons scattered into and scattered out of the line-of-sight. In the presence of scattering, the radiative transfer equation becomes an integral-differential equation. One therefore needs to solve for the whole radiation field simultaneously in order to determine the line-of-sight intensity. However, the radiative transfer equation can be converted to a set of differential equations, under certain approximations, and the equations are solved accordingly with suitable boundary conditions.

A moment method for radiative transfer of scattered emission in the general relativistic setting was proposed by Thorne (1981); another moment method was developed later by Fuerst (2005). The basic principles behind the two methods are similar, with the main difference in the selection of the moment

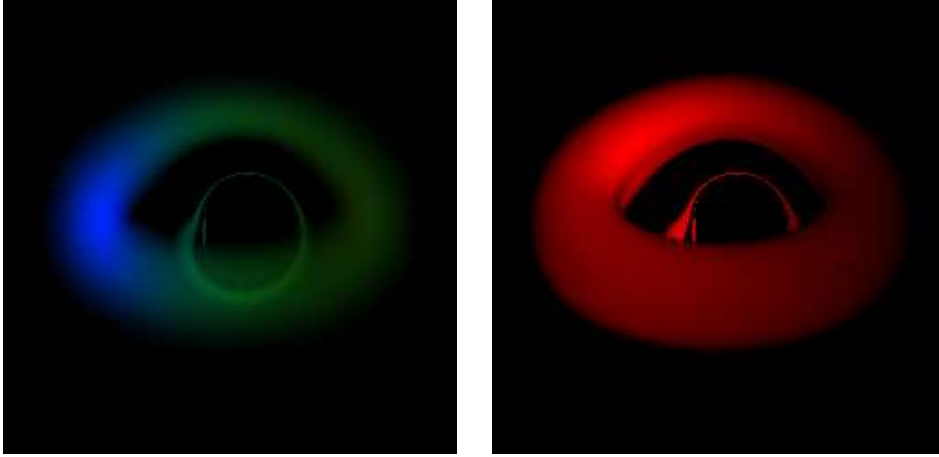


Fig. 10 Left panel: Surface brightness images of an optically thin accretion torus around a Kerr black hole with $a = 0.998$. The view inclination is 60° . The emissivity is contributed by two lines assuming the energies of the Fe $K\alpha$ and $K\beta$ X-ray lines. Absorption is ignored in the radiative transfer calculation. The intensity is arbitrary normalised. Right panel: Surface brightness image of an opaque accretion torus around a Kerr black hole with $a = 0.998$. The viewing inclination is 60° . The intensity is contributed by two lines with Fe $K\alpha$ and $K\beta$ energies and a continuum consisting of thermal free-free component and a power-law component. Absorption are treated explicit in the radiative transfer calculation.

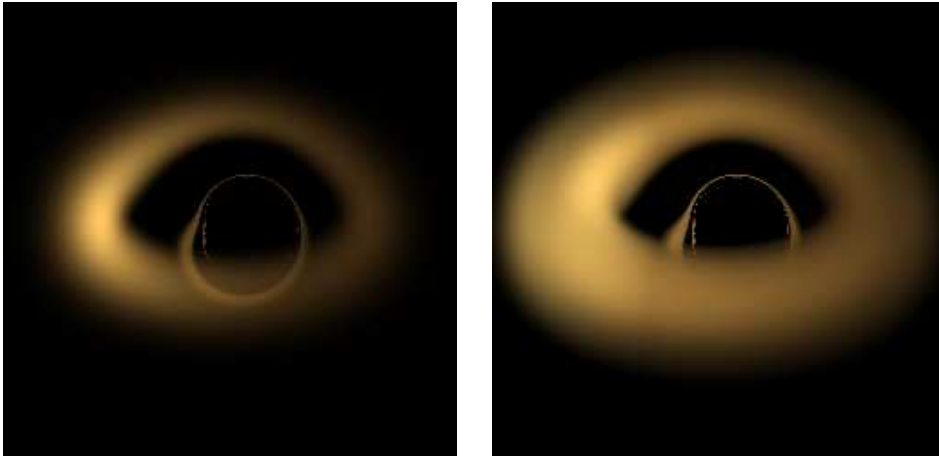


Fig. 11 Surface brightness images of accretion tori around a Kerr black hole with $a = 0.998$ with opacity dominated by scattering. The view inclination is 60° . The opacity is due to free-free emission and electron scattering. The left panel shows a torus with low scattering optical depths; the right panel shows a torus with high scattering optical depths. The central electron number density of the torus takes a value of 5×10^{10} for the case of low optical depths and $2 \times 10^{11} \text{ cm}^{-3}$ for the case of high optical depths. The maximum optical depths in the two cases are roughly 0.1 and 10 in the two cases respectively.

tensors. Here, we give a brief description of the latter method. The technical details, such as derivation of the moment terms ... etc, are presented in Fuerst (2005).

Consider an expansion of the intensity $\mathcal{I}(x^\alpha, k^\alpha)$ in terms of a set of orthogonal symmetric tensors $J_{\alpha_1 \dots \alpha_j}$.

$$\mathcal{I}(x^\alpha, k^\alpha) = a_0 J + \sum_{i=1}^{\infty} a_i J_{\alpha_1 \alpha_2 \dots \alpha_i} n^{\alpha_1} n^{\alpha_2} \dots n^{\alpha_i}, \quad (21)$$

where n^α is the directional unit vector of the photon. From $J_{\alpha_1 \alpha_2 \dots \alpha_i \dots}$ we can generate a set of projected tensors $\mathcal{J}_{\alpha_1 \alpha_2 \dots \alpha_i \dots}$ satisfying the condition $\mathcal{J}_{\alpha_1 \alpha_2 \dots \alpha_i \dots} u^\alpha \propto \mathcal{J}_{\alpha_1 \alpha_2 \dots \alpha_i \dots}$, where u^α is a four-velocity of a preferred reference frame, which may be chosen to be the rest frame of the medium. We can then obtain an approximation by truncating the moment expansion:

$$\mathcal{I}_j(x^\alpha, k^\alpha) = \mathcal{J}_{\alpha_1 \alpha_2 \dots \alpha_j} m^{\alpha_1} m^{\alpha_2} \dots m^{\alpha_j}, \quad (22)$$

where $m^\alpha = n^\alpha + u^\alpha$.

After specifying the absorption and scattering process, we may derive the moment equation explicitly. As an illustration we consider that the opacity is due to free-free emission and electron scattering, with the effective cross sections as σ_{ff} and σ_{T} respectively. The first order moment equation is

$$m_\alpha \left[\mathcal{J}^\alpha{}_{,\beta} n^\beta + \Gamma_{\delta\beta}^\alpha \mathcal{J}^\beta m^\delta + \xi \left(\mathcal{J}^\alpha - \frac{\partial \mathcal{J}^\alpha}{\partial (\ln E)} \right) \right] = -(\sigma_{\text{ff}} + \sigma_{\text{T}}) \rho \mathcal{J}^\alpha m_\alpha + \sigma_{\text{ff}} \rho \mathcal{B} + \sigma_{\text{T}} \rho \mathcal{J}^\alpha u_\alpha, \quad (23)$$

where $\mathcal{B} = B_\nu / \nu^3$, B_ν is the Planck function, and ξ is given by

$$\begin{aligned} \xi &= -\frac{1}{E^2} \frac{DE}{\partial \lambda} \\ &= u^\alpha n_{\alpha;\beta} n^\beta + n^\alpha u_{\alpha;\beta} u^\beta. \end{aligned} \quad (24)$$

The second and higher order moment equations can be derived accordingly. Solving the moment equations yields the tensors $\mathcal{J}_{\alpha_1 \alpha_2 \dots \alpha_j}$, and hence the intensity $\mathcal{I}_j(x^\alpha, k^\alpha)$.

Figure 11 shows images of two accretion tori obtained by the moment calculations. The opacity of the tori is mainly due to electron scattering, and the two tori are examples of low and high scattering optical depths. While an absorption process destroys the line-of-sight photons, scattering causes only energy and momentum redistribution. Thus, without absorption, photons that are generated anywhere in a torus can eventually escape to outside.

Here scattering effects can be seen in the limb. In the cases with absorption (previous sections), the limb itself is manifested as an absorbing layer, but in the scattering case the propagations of the photons are redirected in the limb, i.e. photons can be scattered into the line-of-sight as well as scattered out. In the torus images of Figure 11, the difference in the surface brightness between the limb and the body of the torus is due to the effective free path into the torus where density and temperature are stratified. The surface brightness of the limb is contributed by rays sampling only the cooler surface layer of the torus; the surface brightness of the torus body is contributed by rays penetrating to deeper region where the temperature is higher.

8 SUMMARY AND REMARKS

We have presented a covariant radiative transfer formulation for calculation of emission from accretion disks and tori around black holes. The formulation includes the effects due to internal and external absorption. We have shown that absorption effects can be as important as space-time curvature and relativistic flows in shaping the profiles of the emission lines. Without absorption, an emission line from a geometrically thin opaque relativistic accretion disk will have an asymmetric double-peak profile with a broad red wing and a tall sharp blue peak. In the presence of absorption, the line will lose some of these signatures. In particular, absorption tends to take away the line fluxes at energies red-ward of the line-centre rest-frame

energy. In the severe situations, when the red wing is completely absorbed, the line will appear as if it is a blue-shifted narrow sharp line. Some AGN have been found to show peculiar narrow Fe $K\alpha$ lines centred at energies much higher than their rest-frame energies (e.g. in RXJ J0136.9-3510, Ghosh et al. 2004). Here, we demonstrate that such lines can be produced when there is substantial line-of-sight absorption.

We have shown that geometric effects are important in thick accretion disks (accretion tori). At high viewing inclination angles, the inner surface of a torus, where the emission have the largest energy red-shifts and blue-shifts, can be obscured. As a result, an emission line from an opaque accretion torus will not be as broad as the corresponding line from a geometrically thin accretion disk. Moreover, the line may have a single-peak profile instead, and the line centre is slightly red-shifted. This suggests that asymmetric doubled-peak lines, such as the broad Fe $K\alpha$ line seen in the X-ray spectra of MCG-6-30-15 (Tanaka et al. 1995), probably originate from geometrically thin accretion disks without self-occultation and the line-of-sight absorption is insignificant.

We have generalised the calculations from line spectra to continuum spectra. Our calculations show the edges in the reflection spectra of thin relativistic accretion disks are smeared and shifted. The degree of smearing and energy shifts depend on the viewing inclination of the disk. As the reflection is anisotropic, the contribution of a disk surface element is determined by the pitch angle of the emitting photons that can reach the observer.

We have calculated also the emission from optically thin and semi-opaque accretion tori. Radiative transfer effects, such as the limb effects, as well as relativistic effects, such as boosting, can be seen in the surface brightness images of the accretion tori generated by the calculations.

We have described briefly a new covariant moment formulation (Fuerst 2005) for relativistic radiative transfer in media where scattering processes are important. We apply the formulation to accretion tori with the opacity dominated by electron scattering. Limb effects are shown in the surface brightness images of the accretion tori.

Acknowledgements SVF was supported by an Overseas Research Studentship and a UCL Graduate Research Studentship. KW, KGL and GBR acknowledge the support from the Nuffield Foundation through a Research Bursary program.

References

- Abramowicz M., Jaroszynski M., Sikora M., 1978, *A&A*, 62, 221
 Baschek B., Efi mov G.V., von Waldenfels W., Wehrse R., 1997, *A&A*, 317, 630
 Bowers R., Deeming T., 1984, *Astrophysics I*, Boston: Jones and Barlett
 Dovciak, M., Karas, V., Yaqoob, T., 2004, *ApJS*, 153, 205
 Fabian A.C., Rees M.J., Stellar L., White N.E., 1989, *MNRAS*, 238, 729
 Fabian A.C., Iwasawa K., Reynolds C.S., Young A. J., 2000, *PASP*, 112, 1145
 Fanton C., Calvani M., de Felice F., Cadez A., 1997, *PASJ*, 49, 159
 Fuerst S.V., Wu K., 2004, *A&A*, 424, 733
 Fuerst S.V., 2005, PhD Thesis, University of London
 Ghosh K.K., Swartz D.A., Tennant A.F., Wu K., Ramsey B., 2004, *ApJ*, 607, L111
 Hawley J.F., Balbus S.A., 2002, *ApJS*, 573, 738
 Hölzer G., Fritsch M., Deutsch M., Härtwig J.F., 1997, *Phys. Rev. A*, 56, 4554
 Kozłowski M., Jaroszynski M., Abramowicz M., 1978, *A&A*, 63, 209
 Lindquist R., 1966, *Annals of Physics*, 37, 487
 Lee K.-G., Branduardi-Raymont G., Fuerst S.V., Wu K., Crowley O., 2005, *MNRAS*, to be submitted
 Laor A., 1991, *ApJ*, 376, 90
 Magdziarz, P., Zdziarski A.A., 1995, *MNRAS*, 273, 837
 Martocchia, A., Karas, V., Matt, G., 2000, *MNRAS*, 312, 817
 Reynolds C.S., Young A.J., Begelman M.C., Fabian A.C., 1999, *ApJ*, 514, 164
 Ruszkowski M., Fabian A.C., 2000, *MNRAS*, 315, 223
 Smak J., 1969, *Acta Astronomica*, 19, 155
 Tanaka Y. et al., 1995, *Nature*, 375, 659
 Thorne K.S., 1981, *MNRAS*, 194, 439
 Williams G., 1983, *ApJS*, 53, 523
 Wu K., Soria R., Hunstead R.W., Johnston H.M., 2001, *MNRAS*, 320, 177

DISCUSSION

ALAN MARSCHER: In your calculations, where is the incident continuum coming from to create the reflection spectrum?

KINWAH WU: Our calculations deal with the radiative transfer process. Where the incident continuum comes from is not essential. We have assumed a parametric emissivity law, in which the emissions decrease radially in a power-law form, for the calculations of the emission spectra that I showed. In other words, the origin of the incident continuum to produce the reflection spectrum was not considered in an explicit manner.

MASSIMO CAPPI: Did you introduce the effects due to ionisation (both in the line and continuum) in your code?

KINWAH WU: Our formulation is a generic formulation for general relativistic radiative transfer. The ionisation effects are included as input parameters by means of the absorption and emission coefficients. In other words, the ionisation process was not considered explicitly in our calculations presented here. However, the formulation can take into account the process. What we need are the atomic data to derive the absorption and emission coefficients.

LUCIANO BURDERI: How far outside are the disks and the tori extended in your simulations?

KINWAH WU: First of all, what I showed in my talk are not simulations. They are covariant radiative transfer calculations using a ray tracing method. We considered various disk and torus models. The disks could have outer radii beyond 100 Schwarzschild radius, but those shown here were smaller. The inner radius was taken as the radius of the last stable orbits of the particles. For the tori, the emission surface is determined by the allowable inner radius at the equatorial planes, subject to the velocity/momentum law that we assumed and subject to the equation of state of the gas.